Dimer Disruption and Monomer Sequestration by Alkyl Tripeptides Are Successful Strategies for Inhibiting Wild-Type and Multidrug-Resistant Mutated HIV-1 Proteases[†]

Ludovic Bannwarth,[‡,§,||] Thierry Rose,[*,‡,⊥] Laure Dufau,[§] Régis Vanderesse,[#] Julien Dumond,[§] Brigitte Jamart-Grégoire,[#] Christophe Pannecouque,[▽] Erik De Clercq,[▽] and Michèle Reboud-Ravaux[*,§]

Enzymologie Moléculaire et Fonctionnelle, FRE 2852, CNRS, Université Paris 6 UPMC, Institut Jacques Monod, 2 place Jussieu, 75251 Paris Cedex 5, France, Institut Pasteur, PFBMI, Département de Biologie Structurale, 25 rue du Dr. Roux, 75724 Paris Cedex 15, France, Laboratoire de Chimie Physique Macromoléculaire, UMR 7568 CNRS-INPL, ENSIC 1, rue Grandville, 54001 Nancy, France, and Rega Institute for Medical Research, Katholieke Universiteit Leuven, Minderbroedersstraat 10, 3000 Leuven, Belgium

Received July 30, 2008; Revised Manuscript Received November 12, 2008

ABSTRACT: Wild-type and drug-resistant mutated HIV-1 proteases are active as dimers. This work describes the inhibition of their dimerization by a new series of alkyl tripeptides that target the four-stranded antiparallel β-sheet formed by the interdigitation of the N- and C-monomer ends of each monomer. Analytical ultracentrifugation was used to give experimental evidence of their mode of action that is disruption of the active homodimer with formation of inactive monomer−inhibitor complexes. The minimum length of the alkyl chain needed to inhibit dimerization was established. Sequence variations led to a most potent HIV-PR dimerization inhibitor: palmitoyl-Leu-Glu-Tyr (K_{id} = 0.3 nM). Insertion of D-amino acids at the first two positions of the peptide moiety increased the inhibitor resistance to proteolysis without abolishing the inhibitory effect. Molecular dynamics simulations of the inhibitor series complexed with wild-type and mutated HIV-PR monomers corroborated the kinetic data. They suggested that the lipopeptide peptide moiety replaces the middle strand in the highly conserved intermolecular four-stranded β-sheet formed by the peptide termini of each monomer, and the alkyl chain is tightly grasped by the active site groove capped by the β-hairpin flap in a "superclosed" conformation. These new inhibitors were equally active *in vitro* against both wild-type and drug-resistant multimutated proteases, and the model suggested that the mutations in the monomer did not interfere with the inhibitor.

Human immunodeficiency virus type 1 (HIV-1)[1] protease (HIV-PR) is still a major target for anti-AIDS therapies because of its central role in processing viral enzymes and the essential structural proteins building the virus capsid. Inhibiting HIV-PR results in uninfectious virus (*1, 2*). Protease inhibitors (PIs) are used in combination with reverse transcriptase inhibitors in highly active antiretroviral therapy (HAART) to reduce the virus load and increase the CD4 cell counts in HIV-1-infected patients (*3*). Many inhibitors have been developed that target the active site of this aspartic protease. However, the development of cross-resistance to PIs is a serious limitation in long-term treatment of AIDS patients. Several mutations within and outside the active site of HIV-PR lower the affinity of most of the PIs synthesized by the pharmaceutical industry (*3*). As these PIs are transition state analogues targeting the enzyme active site, the emergence of resistance to one PI may result in cross-resistance to others (*4*). Alternative drug strategies are needed to overcome the risk of resistance developing to these currently available HIV-PR inhibitors. Design of molecules targeting protein oligomer interfaces is a powerful strategy to inhibit properties inherent to protein complexes (*5*).

Several crystallographic structures of HIV-PR have been solved by X-ray diffraction in the absence (free state) and in the presence of inhibitors (bound state) (*6*−*8*). The enzyme is a *C*2-symmetric homodimer, and the catalytic residues D^{25} of both monomers lie close together in the unique active site (Figure 1). The access to the active site is monitored by the β-hairpin flaps (M^{46}−L^{55}) from both subunits held semiclosed in the unbound enzyme and closed in the ligand-bound enzyme (Figure 1). Opening and closure motions upon ligand binding were extensively explored by molecular dynamics (*9*−*11*).

[†] This work was supported by the CNRS and the University Pierre et Marie Curie, Paris VI (UPMC). L.B. held a doctoral fellowship from the MENRS and a short-term grant from the ANRS.

* To whom correspondence should be addressed. M.R.-R.: tel, +33 1 44 27 50 78; fax, +33 1 44 27 59 94; e-mail, michele.reboud@upmc.fr. T.R.: tel, +33 1 45 68 85 99; fax, +33 1 45 68 86 39; e-mail, rose@pasteur.fr.

[‡] L.B. and T.R. contribute equally to this work.

[§] FRE 2852, CNRS, Université Pierre et Marie Curie, Paris 6.

[||] Present address: Yale University School of Medicine, 333 Cedar St., SHM B-386, New Haven, CT 06520.

[⊥] PFBMI, Département de Biologie Structurale, Institut Pasteur.

[#] UMR 7568 CNRS-INPL, Ecole Nationale Supérieure des Industries Chimiques.

[▽] Rega Institute for Medical Research, Katholieke Universiteit Leuven.

[1] Abbreviations: HIV-1, human immunodeficiency virus, type 1; HIV-PR, HIV-1 protease; PI, protease active site inhibitor; C16-YEL, palmitoyl-Tyr-Glu-Leu; A16-YET(0), 2-aminopalmitoyl-Tyr-Glu-thyronine; YET(4), Tyr-Glu-thyroxine.

10.1021/bi801422u CCC: $40.75
Published on Web 12/23/2008

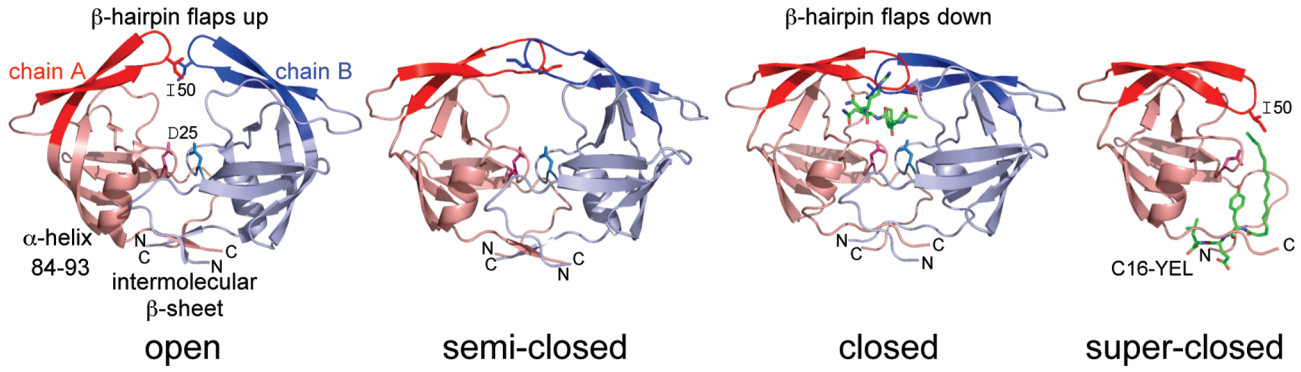

FIGURE 1: Open and closed active site conformations of HIV-PR. The access to the active site (catalytic residues D25) is monitored by the β-hairpin flaps ($M^{46}-L^{55}$ in red and dark blue) from both subunits (chain A in pink/red; chain B in light/dark blue). Crystallographic structures give examples of "open" (1TW7, ligand-free dimer), "semiclosed" (1HHP, ligand-free dimer), and "closed" (1AXA, peptidic inhibitor-bound dimer) conformations. The model built in this work suggested a "superclosed" conformation of C16-YEL inhibitor-bound HIV-PR (monomer). Ligands are shown in atom color-coded sticks. The measurement of the flap opening is given by the distance between I50 and D25 Cα (these residue side chains are shown in sticks): open, 18 Å; semiclosed, 15 Å; closed, 13 Å; and superclosed, 10 Å.

HIV-PR is only active as a dimer with a dissociation constant at equilibrium below 10 nM (*12*). The interface is formed from β-hairpin flaps, helices (residues 84−93), and N- and C-terminal β-strands (Figure 1). The energy of interaction is not regularly distributed along the dimer interface area, and some structurally conserved residues (the "hot spots") secure the binding energy. A four-strand β-sheet, formed by the interdigitation of the C- and N-ends from both monomers, contributes to three-fourths of the total Gibbs free energy of HIV-PR dimerization (*13*). The residues from the N- and C-terminal β-strands are also highly conserved in most HIV-1 isolates, in some HIV-2 isolates, and in drug-resistant HIV-1 variants. Mutations involved in resistance to one or more clinically used PIs lie within or outside the active site but rarely in these β-strands. Targeting this region has led to the development of inhibitors of HIV-PR dimerization (*14*−*17*). This strategy has been successful in other domains such as the disruption of intermolecular β-sheets leading to dislocation of amyloid fibrils responsible for Alzheimer's disease (*18, 19*) and disruption of adhesins from bacterial pili responsible for uropathogenic infections (*20*).

Early studies indicated that peptides mimicking the HIV-PR C-terminus had dimerization inhibitor properties (*21, 22*), and changing the sequence of these interface peptides identified a consensus sequence ISYEL in which the motif YEL is critical (*23*). A long hydrophobic alkyl chain, such as palmitoyl, was then added to the peptide N-terminus to target the cell membrane and help to deliver the inhibitor to the cytoplasm. We have previously suggested that lipopeptides can inhibit the dimerization of wild-type HIV-PR (*24, 25*). The alkyl chain improves the inhibitory potency of interface peptides and switches the mechanism of some of them from competitive inhibition to dimerization inhibition (*24, 25*). Some of them inhibited the virus replication in MT4 assays (*26*). Another class of dimerization inhibitors has a bicyclic guanidinium group between the peptide and lipophilic moieties to compensate for the negatively charged C-terminal carboxylate of F^{99} (*27*). In an attempt to reproduce the antiparallel β-sheet, interface peptides were successfully cross-linked with rigid (*28*−*30*) or flexible (*14, 17, 31*) spacers. The present work describes further studies on structural variations of alkyl tripeptides used as dimerization inhibitors, their mechanism of action, and their efficacy against wild-type and mutated HIV-1 proteases. The observed inhibition constants K_{id} are discussed with reference to molecular models of monomer−inhibitor complexes. We have established the minimum length of the alkyl chain needed to inhibit dimerization, varied the amino acid sequence to improve binding, and introduced D-amino acids to make the molecules more metabolically stable. We used analytical ultracentrifugation to show that the HIV-PR homodimer dissociates to form a lipopeptide−monomer complex. Finally, we have demonstrated that alkyl tripeptides inhibit multidrug-resistant mutated HIV-1 proteases.

EXPERIMENTAL PROCEDURES

Inhibitor Synthesis and Evaluation of Metabolic Stability. Peptides and lipopeptides were synthesized and purified as described previously (*32*) and detailed in Supporting Information (SD1). The metabolic stability of inhibitors was evaluated in RPMI culture medium containing 20% fetal calf serum by assaying their breakdown after 48 h at 37 °C using HPLC analysis (*30*).

Wild-Type and Mutated Proteases. The four PR mutants, D30N, I50V, V82A, and G48V/L90M, were constructed with the QuickChange site-directed mutagenesis kit (Stratagene, La Jolla, CA) using appropriate pairs of primers (Proligo, Paris, France). The plasmid pET9PRWT bearing the wild-type sequence of the protease gene from the HIV (BRU) DNA clone (subclone of λJ19) was used as template for the PCR amplification cycles. The resulting mutated plasmids were sequenced (Genome Express, Meylan, France) on both coding and noncoding strands. WT PR and D30N, I50V, V82A, G48V/L90 M mutants and multimutated MDR-HM (*33*) and ANAM-11 (*34*) (Prof. E. Freire, The Johns Hopkins University, Baltimore, MD) were expressed in *Escherichia coli* BL21(DE3) rosetta pLysS strain (Novagen, Darmstadt, Germany), purified, and refolded according to Billich et al. (*35*).

Enzyme and Inhibition Assays. The fluorogenic substrate DABCYL-γ-abu-SQNYPIVQ-EDANS (DABCYL, 4-(4′-dimethylaminophenylazo)benzoyl; γ-abu, γ-aminobutyric acid; EDANS, 5-[(2-aminoethyl)amino]naphthalene-1-sulfonic acid) was purchased from Bachem (Voisin-le-Bretonneux, France). Fluorescence intensities were measured in a spectrofluorometer Perkin-Elmer LS 50B (Norwalk, CT)

(slits 10 nm; cuvette volume of 500 μL) and absorbance in an Uvikon 941 spectrophotometer (Kontron, Zurich, Switzerland).

The proteolytic activities of WT-PR and mutated proteases were determined fluorometrically ($\lambda_{ex} = 340$ nm; $\lambda_{em} = 490$ nm) in 100 mM sodium acetate, 1 mM EDTA, and 1 M NaCl at pH 4.7 and 30 °C (*30*). Some kinetics were performed in 0.1 M NaCl for comparison, but experiments were routinely performed in 1 M NaCl; the enzyme was stabilized by the high ionic strength (*36*). The substrate and the compounds were first dissolved in DMSO. The final DMSO concentration was kept at 3% (v/v). The mechanism of inhibition and the corresponding kinetic constants K_{ic} (competitive inhibition) and/or K_{id} (dimerization inhibition) were determined using Zhang-Poorman kinetic analysis (*37*). Kinetic experiments were carried out at constant substrate concentration (5.2 μM) and at least four enzyme concentrations (3.5−31.7 nM). Inhibitor concentrations were 1 and 2 μM for C6-YEL, 0.28 and 1 μM for C8-YEL, 0.28 and 0.42 μM for C10-YEL, 0.14 and 0.28 μM for C12-YEL, 0.28 and 1 μM for C14-YEL, 3 and 5 μM for C16-LEY, 1 and 2 μM for C16-yel, and 4 and 6 μM for C16-ley. The experimental data were fitted according to ref *37*. All experiments were performed at least in triplicate. The influence of pH on the inhibitory capacity of C16-YEL was analyzed using acetate buffers at pH 4.7, 4.9, 5.1, 5.3, 5.5, 5.7, 5.9, and 6.1 (100 mM sodium acetate, 1 mM EDTA, and 1 M NaCl).

Analytical Ultracentrifugation. Sedimentation experiments were performed at 20 °C on a Beckman-Coulter Optima XL-I analytical ultracentrifuge (Fullerton, CA) using a four-hole rotor (AN-60 Ti) with absorbance and optical interference acquisition systems. Protein samples were dialyzed against the following buffer: 50 mM sodium acetate, pH 4.7, 100 mM NaCl, 0.1 mM EDTA, and 3% (v/v) DMSO. The same buffer was used to dilute samples and as a blank in the two-sector aluminum cells with sapphire windows (path length 1.2 cm).

The homogeneity of the protein solution and the sedimentation coefficient s of molecular species were evaluated by processing sedimentation velocity experiments at 60 krpm in 150 μL samples prepared at three HIV-PR/C16-YEL ratios (1:0, 1:0.5, 1:1) in the same run with a constant protein concentration (8 μM). We recorded 200 interference optical and absorbance (280 nm) scans. The theoretical boundaries from continuous discrete and noninteracting species were fitted to experimental data profiles with the software Sedfit (*38*) based on a finite element solution of Lamm's equation. This gave the distribution $c(s)$ of sedimentation coefficients s between 0.1 and 20 S of populated molecular species. The one or two first scans were excluded if unexpected features were noticed (increased absorbance at the meniscus shoulder and waves at the plateau) due to high molecular weight aggregates (>20 S). This improved the fits of sedimentation of low molecular weight species (<20 S). We used a confidence level of 0.95 for the regularization procedure. The frictional ratio f/f_0 was adjusted to reflect the theoretical MW in first approximation; then the experimental values for the molecular weight of the single species were measured by sedimentation equilibrium.

We evaluated weights of molecular species by sedimentation equilibrium experiments at four speeds (20, 22, 24 and 26 krpm) in 40 μL samples prepared at seven HIV-PR/C16-YEL ratios (1:0, 1:0.2, 1:0.5, 1:1, 1:2, 1:5, and 0:5) with a constant protein concentration in six of them (8 μM) using a eight-hole rotor AN-50 Ti. The equilibrium status was checked for each speed by comparing scans (280 nm, 0.001 cm steps, absorbance values averaged from 10 successive measurements) every 15 min from 60 to 120 min for the 40 μL samples. Equilibrium was usually reached after 90 min. We verified that scans acquired at 90, 105, and 120 min were identical; we then recorded seven supplementary scans to make a series of ten scans per speed. After the acquisitions at 20, 22, 24, and 26 krpm, we checked the absorbance of samples at the meniscus at 50 krpm, the maximal speed for an eight-hole Ti rotor, as most of the HIV-PR had been cleared to the cell bottom. Forty absorbance scans (10 scans/speed, four speeds 20, 22, 24, 26 krpm) were fitted together with the software Origin 6.0 (Microcal, Northampton, MA) using the theoretical distribution of the concentration of single or self-associating ideal species $c(r)$ against the radial distance to the rotor axis r:

$$c(r) = \sum_{n=1-4}[(c_{\text{monomer},r0})^n K_{a,n} \exp(nM(r^2 - r_0^2) \times (1 - \nu\text{-}bar\rho)\omega^2/RT)] + B$$

where $c_{\text{monomer},r0}$ is the concentration of the monomer at the meniscus r_0, the number of subunits n, the association constant $K_{a,n}$ with $K_{a,1} = 1$ and $K_{a,n} = c_{n\text{-mer}}/[c_{\text{monomer}}]^n$), the specific partial volume $\nu\text{-}bar$, the solvent density ρ, the angular velocity ω, the gas constant R, the temperature T, and the offset B fixed at the average of the absorbance values at the meniscus from the scans recorded at 50 krpm. Variances between experimental points and best fits were used to select the models: single (all-monomer or all-dimer) or self-associating ideal species (monomer−dimer equilibrium).

The specific partial volume, theoretical molecular weight, and molar extinction coefficients at 280 nm of HIV-PR were computed from the protein sequence: $\nu\text{-}bar = 0.743$ mL/g, MW = 10720 Da, and $\epsilon^{280} = 12600$ M^{-1} cm^{-1}; C16-YEL $\nu\text{-}bar = 0.762$ mL/g, MW = 662 Da, and $\epsilon^{280} = 1280$ M^{-1} cm^{-1}. The solvent density and viscosity were calculated with the Sednterp software (Hayes DB, Laue T, and Philo J): $\rho = 1.004$ g/mL and $\eta = 0.0012$ Pa·s.

Molecular Modeling. The HIV-PR−lipopeptide complex was modeled in four steps detailed in the Supporting Information (SD4). We first built a HIV-PR/C16-YEL model from crystallographic data for the dimer (1AXA, resolution 2.0 Å (*7*). (1) We replaced the monomer B C-terminus with C16-YEL. (2) We then evaluated the flexibility of monomer A loops from restrained molecular dynamics (Discover, Accelrys, San Diego, CA) and selected normal modes (NOMAD-ref (*39*)) that might enhance lipopeptide binding. (3) We ranked the models of the complex according to stereochemical and energy criteria and optimized the best model HIV-PR/C16-YEL. (4) We compared the binding of inhibitor series and HIV-PR single and multiple mutations.

HIV-PR/inhibitor interface area, ΔASA, was estimated by computing the solvent accessibility surface area (SASA) using a 1.4 Å probe radius:

$$\Delta\text{ASA} = \text{ASA}_{\text{HIV-PR}} + \text{ASA}_{\text{inhibitor}} - \text{ASA}_{\text{HIV-PR/inhibitor}}$$

Table 1: Structure of Peptide Compounds and *in Vitro* Inhibition of Wild-Type and Mutated Proteases

HIV-1 proteases[a]	inhibitors[b]	K_{id} (nM)[c]	K_{ic} (nM)[d]
wild type	C16-YEL[e]	11	
	C14-YEL	9	
	C12-YEL	21	
	C10-YEL	14	594
	C8-YEL	44	1300
	C6-YEL		1240
	C16-LEY	0.3	
	C14-LEY	14	
	C12-LEY	150	150
	C16-YDL	67	
	C16-YET(0)[e]	10	
	C16-YET(4)[f]	20	
	A16(1)-YET(4)[f]	10	
	A16(2)-YET(4)[f]	5	
	C16-yel	400	
	C16-ley	1100	
	C16-LeY	17	
	C16-yET(0)	80	
	YEL[e]	2350	
	yel	11300	
V82A	C16-YEL	124	
D30N		94	
I50V		60	
G48V/L90M		46	
MDR-HM	C16-YEL	35	
	C14-YEL	11	
	C12-YEL	42	
	C16-LEY	17	
ANAM-11	C16-YEL	81	
	C14-YEL	6	
	C12-YEL	13	
	C16-LEY	6	

[a] Wild-type and mutated proteases. [b] Inhibitor series: C16 indicates the number of carbons in the linear alkyl chain, C16-YEL corresponds to palmitoyl-YEL or CH_3-$(CH_2)_{14}$-CO-YEL; A16 corresponds to 2-amino-palmitoyl, A16(1) and A16(2) enantiomers, T(0) to L-thyronine, T(4) to thyroxine. Amino acids: D (lower case letter), L (capital letter). [c] Inhibition constant for dimerization at pH 4.7 and 30 °C; standard errors of initial rates are less than 5%. [d] Inhibition constant for active site inhibition at pH 4.7 and 30 °C; standard errors are less than 15%. [e] Reference *24*. [f] Reference *25*.

The polar and apolar fractions of interface areas were computed from N and O (polar) and C and S (apolar) atom contributions to SASA.

RESULTS

Lipotripeptides with C14 and C16 Alkyl Chains Are the Most Potent Dimerization Inhibitors. We synthesized a new series of lipopeptides having alkyl chains of different lengths and different amino acid sequences listed in Table 1. C16-YEL produced identical inhibitions of HIV-PR when assayed in either 0.1 M NaCl or 1 M NaCl. Raising the NaCl concentration stabilized the protease (*36*). The mechanism of HIV-PR inhibition was assessed at 1 M NaCl, pH 4.7, and 30 °C using Zhang−Poorman kinetic analysis (*37*): plots of $[E]_0/\sqrt{v_i}$ vs $\sqrt{v_i}$ are constructed to discriminate between the inhibition of dimerization alone (parallel lines), competitive inhibition (altered slopes and unaltered *y*-axis intercepts), and mixed inhibition (altered slopes and altered *y*-axis intercepts) (Figure 2). We determined the minimum and optimum lengths of the lipotripeptide alkyl chain required to inhibit HIV-PR dimerization (Table 1). Both the type of HIV-PR inhibition and the inhibitory potency were affected by the length of the alkyl chain of CH_3-$(CH_2)_n$-CO-YEL and CH_3-$(CH_2)_n$-CO-LEY. The best dimerization inhibitors were

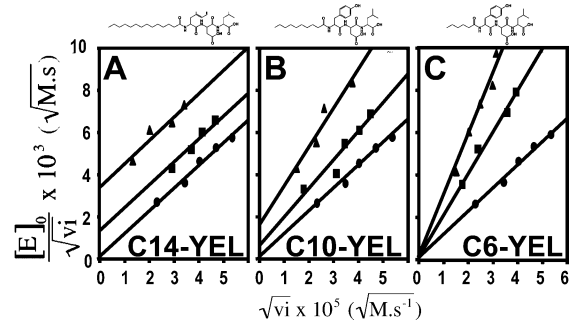

FIGURE 2: Influence of the alkyl chain length on dimerization inhibition. Zhang−Poorman plots are displayed for the inhibition of HIV-PR by compounds C14-YEL (A), C10-YEL (B), and C6-YEL (C) at pH 4.7 and 30 °C. HIV-PR activity was measured at the following inhibitor concentrations: 133 nM (■) and 400 nM (▲) for C14-YEL; 11 nM (■) and 33 nM (▲) for C10-YEL; 500 nM (■) and 1500 nM (▲) for C6-YEL. Activity was also measured without inhibitor (●). The straight lines were fitted to the data by linear regression. Ligand structures indicated above corresponding plots are detailed in Supporting Information (SD2).

obtained with C14 ($n = 12$) and C16 ($n = 14$) alkyl chains. C10 ($n = 8$) and C8 ($n = 6$) alkyl chains resulted in mixed inhibition, while the shorter C6 ($n = 4$) alkyl chain gave competitive inhibition (Figure 2). The peptide moiety LEY with a C12 alkyl chain produced mixed inhibition whereas C12-YEL was a dimerization inhibitor (Table 1).

C16-LEY Is the Best Inhibitor, and Large C-Terminal Groups Are Favored. It has been suggested that the peptide moiety of C16-YEL might replace the β-strand L^{B97}-N^{B98}-F^{B99} of monomer B between the two N- and C-terminal β-strands of monomer A as displayed in the HIV-PR crystal structure (*24, 25*). This is corroborated by the fact that C16-LEY, whose peptide sequence is more similar to the HIV-PR C-terminus sequence LNF than is C16-YEL, is an even more potent inhibitor ($K_{id} = 0.3$ nM) than C16-YEL ($K_{id} =$ 11 nM) (Table 1). The inhibition by lipopeptides is not affected when C-terminal residues have a larger side chain than Y like the nonproteogenic residues thyronine T(0) and thyroxine T(4) (Table 1). The action of the inhibitor was also studied under pH conditions where HIV-PR is effective for Gal-Pol processing (*40*). At a fixed inhibitor concentration (1.41 μM), the inhibition remained fairly constant (50−61%) when the pH was increased by 0.2 pH unit from 4.7 to 6.1. Assuming a pK_a of 4.3 for E, the protonated fraction represents 28% at pH 4.7 and 1.5% at pH 6.1. This is in agreement with the inhibitory capacity of the unprotonated form of C16-YEL.

Substitutions of L-Amino Acids by Their D-Counterparts at the First and Second Positions Do Not Affect the Inhibition Potency of Lipotripeptides. One way to increase the metabolic stability of lipopeptides is to incorporate D-amino acids. The half-life of C16-YEL is 19 h at 30 °C in RPMI culture medium containing 20% fetal calf serum, while the lipopeptide containing D-amino acids, C16-yel, was not hydrolyzed under the same conditions. The tripeptide yel containing three D-amino acids and no alkyl chain was a poorer inhibitor of dimerization (5-fold) than the peptide YEL containing three L-amino acids (Table 1). Adding a palmitoyl group to the tripeptide N-end increased its activity by a factor of 213 for C16-YEL, but by only 28 for C16-yel. Nevertheless, C16-yel ($K_{id} = 400$ nM) was 36-fold less efficient than C16-YEL ($K_{id} = 11$ nM), while C16-ley ($K_{id} = 1100$ nM) was

Table 2: Comparison of Inhibition Ratios of HIV-1 Mutated Proteases versus Wild Type for Alkyl Peptides and Clinical PIs

HIV-1 proteases[a]	inhibitors[b]	$K_{id(mut)}/K_{id(wt)}$[c]	$K_{ic(mut)}/K_{ic(wt)}$[d]
V82A	C16-YEL	11	
	ritonavir		15
D30N	C16-YEL	8.5	
	nelfinavir		6
I50V	C16-YEL	5.4	
	amprenavir		83
G48V/L90M	C16-YEL	4	
	saquinavir		1000
MDR-HM	C16-YEL	3.2	
	C14-YEL	1.2	
	C12-YEL	2	
	C16-LEY	56	
	nelfinavir		210
	amprenavir		85
	indinavir		200
	saquinavir		2000
	ritonavir		1500
ANAM-11	C16-YEL	7.3	
	C14-YEL	0.7	
	C12-YEL	0.6	
	C16-LEY	23	
	nelfinavir		2840
	indinavir		2030
	saquinavir		4200
	ritonavir		78000

[a] Mutated proteases. [b] Inhibitor series. [c] Ratio between dimerization inhibition constants for mutated and wild-type HIV-1 proteases. [d] Ratio between active site inhibition constants for mutated and wild-type HIV-1 proteases (*30*).

3700-fold less efficient than C16-LEY (K_{id} = 0.3 nM) (Table 1). Therefore, efficient dimerization inhibitors are obtained by substituting a single position: C16-yET(0) (K_{id} = 80 nM) is only 8-fold less potent than C16-YET(4) (K_{id} = 10 nM) and C16-LeY 55-fold less so than C16-LEY (Table 1).

C16-YEL and C16-LEY Inhibit Efficiently Multidrug-Resistant Mutated HIV-1 Proteases. We produced single-point and double-point mutated proteases that preferentially affect a single PI, such as D30N (nelfinavir), V82A (ritonavir), I50V (amprenavir), and G48V/L90 M (saquinavir), and two multimutated proteases ANAM-11 and MDR-HM, analogous to the proteases found in multidrug-resistant mutants. ANAM-11 (L10I-M36I-S37D-M46I-R57K-L63P-A71V-G73S-I84V-L90M-I93L) has eleven mutations (*34*), and MDR-HM (L10I-M46I-I54V-V82A-I84V-L90M) has six mutations (*33*), only one (I84V) or two (V82A, I84V) of which lie in the active site. These mutations make clinically used PIs less active than they are against the wild-type HIV-PR, as indicated in Table 2. The $K_{i,mut}/K_{i,wt}$ ratios vary from 6 (D30N/nelfinavir) to 78000 (ANAM-11/ritonavir), indicating a significant increase in the inhibition constant (Table 2). Remarkably, C16-YEL and C16-LEY inhibited the dimerization of all the mutated proteases described above (Table 2). The inhibitory potencies against these mutated proteases were either greater than their potencies against the wild-type protease, the same, or only a little lower (1.2−12-fold). Finally, C16-YEL is 14−87-fold more potent *in vitro* against ANAM-11 than clinical anti-proteases.

Ultracentrifugation Gave Clear Evidence That C16-YEL Dissociates the HIV-PR Dimer and Sequesters Monomers. We used analytical ultracentrifugation to demonstrate the noncovalent dissociative mechanism by which C16-YEL acts. Sedimentation velocity experiments were run to estimate the homogeneity of molecular species in a series of

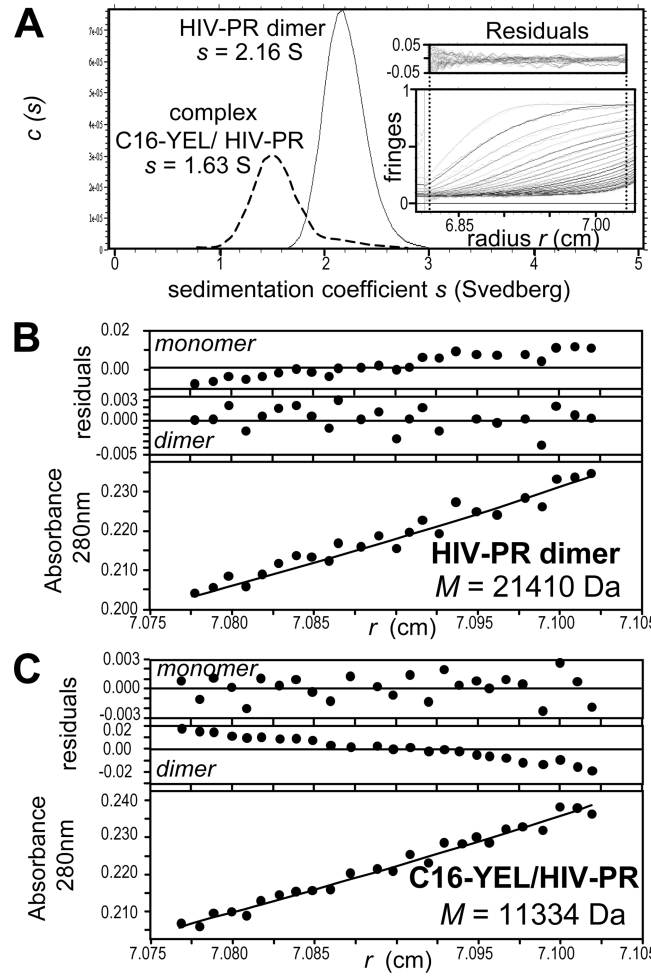

FIGURE 3: Analytical ultracentrifugation. Sedimentation velocity. (A) Optical interference scans were plotted in the inset for HIV-PR at 8 μM (300 μL), 20 °C, 60 krpm. Interference fringes are plotted against the distance from the rotor axis, and theoretical boundaries are shown in thick lines. Residuals between experimental data and theoretical values are plotted against the distance from the rotor axis in the inset top panel. The best fits of the sedimentation coefficient distribution $c(s)$ with the experimental data for HIV-PR alone at 8 μM (lines) and for a 1:1 mix HIV-PR/C16-YEL (dashed). The sedimentation coefficients of main peaks are indicated as best friction ratios f/f_0 when the MW was set as close as possible to that of the monomer/ligand complex or the dimer. Sedimentation equilibrium (B, C). One representative absorbance scan from a data set of 40 used for the analysis (10 scans × 4 speeds, total 1200 data points) was plotted after reaching equilibrium (90 min) for HIV-PR alone at 8 μM (panel B) and a 1:1 mix HIV-PR/C16-YEL (panel C), 40 μL, 20 °C, 20 krpm. Absorbances are plotted against distance r from the rotor axis. Residuals with monomer and dimer theoretical models are plotted, and the best fit is indicated as a solid line.

protein−inhibitor solutions. Interference optics scans of the HIV-PR (8 μM) in the absence of inhibitor at 20 °C were fitted to the theoretical boundaries of a continuous distribution of discrete and noninteracting species. The sedimentation coefficient distribution $c(s)$ (Figure 3A) was that of a single molecular species ($s_{20,w}$ = 2.16 S) which is consistent with a homodimer of theoretical MW 21440 Da. The sedimentation of a HIV-PR plus C16-YEL mixture (mol/mol ratio 1:1) showed a main peak with a $s_{20,w}$ of 1.65 S, corresponding to the HIV-PR monomer, and minor broad peaks above 10.0 S, indicating the presence of aggregating species. The shallow tail at the right of the major peak (1.65 S) might also result of the protease aggregation propensity.

As long equilibrium sedimentation experiments at 20 °C gave strong signs of HIV-PR aggregation, we worked with small sample volumes, 40 μL, which provided fewer data points (~30 points/scan) but required less time to reach equilibrium (90 min). The best fit of the whole absorbance scan set from 20 to 26 krpm (1200 data points per sample) was with a homodimer of HIV-PR considered as a single species at 8 μM (MW = 21410 Da; variances with a monomer model 2.72×10^{-5}, a dimer model 0.69×10^{-5}, a monomer−dimer equilibrium model 0.67×10^{-5}; Figure 3B) and with a complex C16-YEL/monomer HIV-PR considered as a single species for the 1:1 ratio mixture of the two molecules at 8 μM (MW = 11334 Da; variance for a monomer model 0.53×10^{-5}, dimer 2.68×10^{-5}, monomer−dimer 0.53×10^{-5}; Figure 3C). C16-YEL/HIV-PR sedimentation data did not fit better the self-associating species model than the single species model. Thus there was no evidence of monomer−dimer equilibrium at the C16-YEL and HIV-PR tested concentrations (8 μM) confirming that the tail observed in sedimentation velocity might result of the protease aggregation rather than monomer−dimer equilibrium. The calculated MW from the best fit of C16-YEL/HIV-PR data compared well with the predicted molecular weight of 11294 Da for a monomer including the bound inhibitor. Absorbance scans were also acquired at protease−inhibitor ratios from 1:0.2 to 1:5, keeping the protease concentration constant (8 μM). The population of dimeric species decreased as the inhibitor concentration was increased (Supporting Information SD3.C), indicating that C16-YEL behaved as a dissociative inhibitor and sequestered HIV-PR monomers. Sedimentation velocity and sedimentation at equilibrium experiments showed that C16-LEY (8 μM) and C12-YEL (8 μM) also bound to HIV-PR monomers (8 μM) and formed 1:1 ratio complexes ($s_{20,w}$ of 1.61 and 1.63 S, respectively) and behaved as C16-YEL (Supporting Information SD3).

Models of the Inhibitor/HIV-PR Complex Corroborate Kinetics with an Optimal Occupancy of the Hydrophobic Enzyme Cleft by the C16 Alkyl Chain. In the model of the C16-YEL/HIV-PR complex, the wide cleft in monomer A where the helix R^{B87}−G^{B93} of monomer B usually sits (Figure 4A) is narrowed by the closure of loops T^{A4}−P^{A9}, L^{A24}−D^{A30}, I^{A66}−K^{A70}, and the β-hairpin flap M^{A46}−K^{A55} over the alkyl chain. The cleft grasps the ligand tightly, which buries several hydrophobic side chains from the cleft floor (L^{A24}, I^{A84}), the adjacent loops (I^{A47}, I^{A50}, I^{A54}, V^{A82}), and covering the catalytic residue D^{A25} (Figure 4B). The flap opening measured by the distance $C\alpha D^{A25}$−$C\alpha I^{A50}$ is much more closed over the cleft filled by C16-YEL (10 Å) in this "superclosed" model than in the closed crystallographic dimer (13 Å) as shown in the Figures 1 and 4C. This flap also buries hydrophobic residues V^{A32}, V^{A56}, V^{A75}, and L^{A76}. We noticed that the side chains of W^{A6} and F^{A99} are closer to each other, partially burying the alkyl chain (C1−C4) of C16-YEL. This corroborates the observation of the increased signal of W^{A6} from the HIV-PR T26A mutant measured by NMR HSQC when the ligand acetyl-SYEL is added (*41*). The other side of the alkyl moiety (C1−C6) is protected from solvent by L^{A97} and by Y^1 of the tripeptide itself. The tight fit of the ligand in the cleft excludes most water molecules from around the hydrophobic residues of the HIV-PR active site, thus optimizing the interface area. As a consequence of the cleft filling, the solvent-accessible surface area (SASA) of the complex HIV-PR/C16-YEL (5793 Å^2) is smaller than the HIV-PR monomer SASA (6185 Å^2). The HIV-PR interface with C16-YEL, $\Delta ASA_{HIV\text{-}PR/C16\text{-}YEL}$ = 1347 Å^2, is composed of 33.6% polar and 66.4% apolar contributions. The interface $ASA_{HIV\text{-}PR/YEL}$ of the peptide moiety YEL contributes 68% of the C16-YEL interface $ASA_{HIV\text{-}PR/C16\text{-}YEL}$ but only 54% of the apolar contribution, suggesting that the alkyl chain is an important contributor to the entropy of the inhibitor binding free energy.

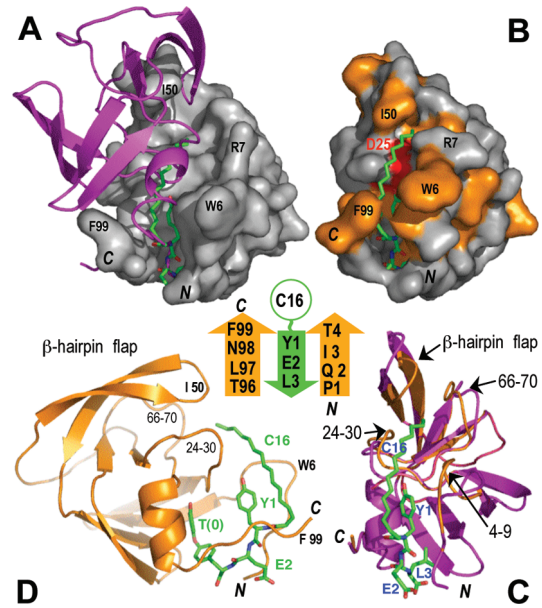

FIGURE 4: Models of alkyl peptide/HIV-PR complexes. (A) C16-YEL backbone replaces the HIV-PR C-terminal β-strand in the dimer, and the palmitoyl chain competes with the dimer helix. The solvent-accessible surface of monomer A from the crystallized dimer (1AXA (*7*)) is shown in light gray, and the backbone of monomer B is shown as a purple sketch. The C16-YEL from the model of the alkyl tripeptide/monomer complex is shown as color-coded sticks when the protease backbone is superimposed on monomer A of the crystallized dimer. (B) The protease monomer tightly grasps the alkyl chain moiety which buries most of protease hydrophobic side chains. In the C16-YEL/monomer model, the solvent-accessible surface of the protease is shown in gray, hydrophobic residues are in orange, the catalytic D^{25} is in red. C16-YEL is shown as a stick model. (C) Loops and flap motions improve C16-YEL binding. The structure sketches of the monomer A backbone from the dimer (1AXA) in purple and the monomer from the C16-YEL/protease model in orange are superimposed. C16-YEL (in green) is shown as a stick model. The central sketch shows the antiparallel intermolecular β-strands color-coded as the model. (D) Large side chains as thyronine (T(0)) and thyroxine (T(4)) can occupy the "F^{99} pocket". Left side view of the C16-YET(0) (sticks)/protease (orange sketch) complex (90° rotation of the HIV-PR monomer from the front view C).

Protease−ligand models were built for alkyl lengths from C2 to C26. The longest alkyl chain that can fit into this "superclosed" model is C17, while the longest alkyl chain that fits into the closed model is C21. The catalytic side chain D^{25} in the cleft is accessible for C10 and longer alkyl chains (detailed in the Supporting Information SD5).

Models Are Consistent with Kinetic Data for Alkyl Tripeptides Incorporating D-Amino Acids or Large Moieties. The backbone of the tripeptide is intercalated between the two HIV-PR β-strands P^{A1}−T^{A4} and T^{A96}−F^{A99} sketched in Figure 5. The Y^1 side chain of C16-YEL extends the cleft floor fitting the alkyl chain. The E^2 side chain points toward

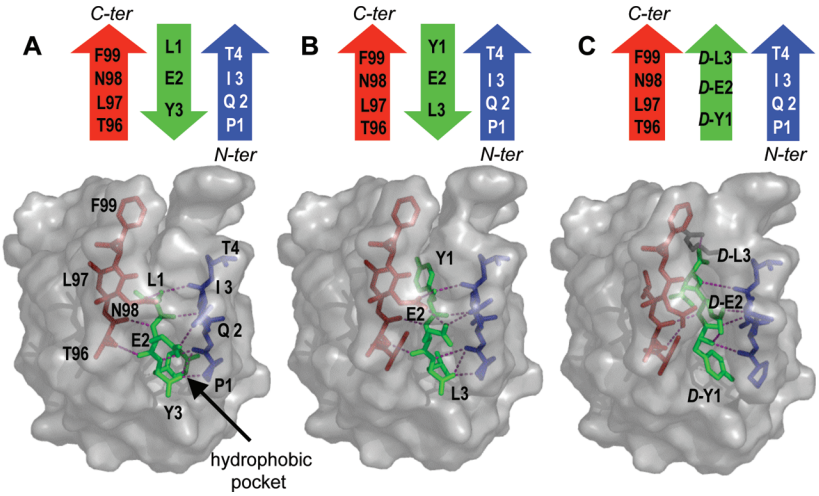

FIGURE 5: Models of the complexes YEL/protease and yel/protease. The YEL backbone forms an antiparallel β-sheet and the yel backbone a parallel sheet, both intercalated between the monomer N- and C-terminal β-strands. The solvent-accessible surface of HIV-PR is shown as a transparent gray skin over the N- (blue) and C-terminal strands (red). Tripeptides LEY (A), YEL (B), and yel (C) are indicated in green, and the H-bond network is in purple to illustrate sheet architectures: N−C directions of strands are indicated above with corresponding colors. Y^1 in YEL/protease and y^1 (D-Y1) in yel/protease occupy different pockets. The F^{99} hydrophobic pocket that accommodates the C-terminal F99 from chain B in the dimer is indicated by the arrow.

the solvent, H-bound to Q^{A2}. The L^3 side chain is embedded in a pocket deeply buried within the PR core, which is usually occupied by F^{B99} in the homodimer (F^{99} pocket). We explored the effects of changing these residues, assuming that all the derivatives occupy the same binding site on HIV-PR as C16-YEL, with local rearrangement reached by minimization. C16-$L^1E^2Y^3$ is the most potent inhibitor; its sequence is very close to that of $L^{B97}N^{B98}F^{B99}$ in the HIV-PR C-terminal β-strand. The L^1 side chain is large enough to reach and prolong the hydrophobic cleft floor: it also protects the alkyl chain from water molecules. The Y^3 side chain is embedded in the HIV-PR deep internal pocket, optimizing contacts with the hydrophobic side chains from I^{A3}, I^{A24}, and L^{A90} by excluding water molecules from their vicinity. The replacement of Y^3 with the residues thyronine or thyroxine increases the occupancy of the F^{99} hydrophobic pocket, removing most of the putative open spaces for water molecules (Figure 4D).

The residues of C16-$Y^1E^2L^3$ were replaced with D-amino acids (C16-$y^1E^2L^3$, C16-$L^1e^2Y^3$, C16-$y^1e^2l^3$, C16-$l^1e^2y^3$). Kinetic analysis indicated that such substitutions are unfavorable at the third position, mostly due to steric hindrance and have moderate effects at the first and second positions (Table 1). Puzzlingly, K_{id} for C16-ley is 3666-fold larger than that for C16-LEY, whereas the C16-yel K_{id} is only 36 times larger than that of C16-YEL. Comparison of models of the complex indicates that the D-L^3 side chain of C16-yel is more easily accommodated than that of the D-Y^3 of C16-ley. The K_{id} for yel is only 28 times larger than that of C16-yel, whereas the K_{id} of YEL is 213 times larger than that of C16-YEL. Comparison of results after several modeling trials using distinct orientations of the peptide strand or frame shift of interstrand H-bond network suggests that the peptide strand yel is advantageously oriented in the opposite direction than YEL, making a parallel intermolecular β-sheet (L-strand/D-strand/L-strand) instead of an antiparallel β-sheet (Figure 5). This conformation places the side chain of D-Y^1 in the hydrophobic pocket instead of that of D-L^3, the D-E^2 carboxyl oxygen H-bound with N^{A2} amine and the yel C-terminal carboxyl oxygen ion-paired with the R^{A9} guanidinium amine. Thus the C16-yel palmitoyl chain is pointing in a less favorable environment than C16-YEL palmitoyl that snugly sits in the hydrophobic cleft. C16-ley and ley peptide strands should be oriented as C16-YEL.

The substitutions of L-amino acids by their D-counterparts at the first and second positions do not affect the superimposition of the C16-yEL and C16-YeL over C16-YEL. Conversely, replacing the third position residue with a D-amino acid compromises binding, as indicated by the kinetics and the model C16-YEl/HIV-PR. Replacing the residues in all three positions by D-amino acid favors the opposite arrangement of β-strand in the HIV-PR N- and C-terminal β-sheet (Figure 5).

Multiple Mutations Do Not Interfere in Models with the Binding of Alkyl Tripeptides to the Enzyme, in Agreement with the Kinetic Analysis. Single (D30N, G48V, I50V, V82A, L90M), double (G48V/L90M), and multiple mutations (MDR-HM and ANAM-11) all affect the binding of PIs to HIV-PR dimers (Table 2). However, they do not affect the binding of C16-YEL (Figure 6) held through its backbone by a hydrogen bond network away from the active site and by the flexible alkyl chain that can easily compensate mutated chain steric hindrance by sitting more or less high in the active site cleft. V82A opens a hole in the hydrophobic cluster assembling the flap residues (I^{A50}), the cleft floor (I^{A84}), and the terminal methyl from C16. This mutation decreases the inhibition potency of C16-YEL about 11-fold.

DISCUSSION

New HIV-PR inhibitors are urgently needed to overcome the drug-resistance problem of HIV strains and circumvent the high occurrence of HIV-PR sequence mutations in long-term treatment of AIDS patients with PIs. Considerable efforts have been made to find alternative inhibitors that avoid the cross-resistance observed with inhibitors targeting the HIV-PR active site (saquinavir, indinavir, ritonavir, nelfinavir, amprenavir, lopinavir, atazanavir, fosamprenavir, tipranavir, and darunavir). Peptides mimicking the HIV-PR C-terminus disrupt enzyme homodimers, thus opening new strategies for inhibiting protease activity. The recently

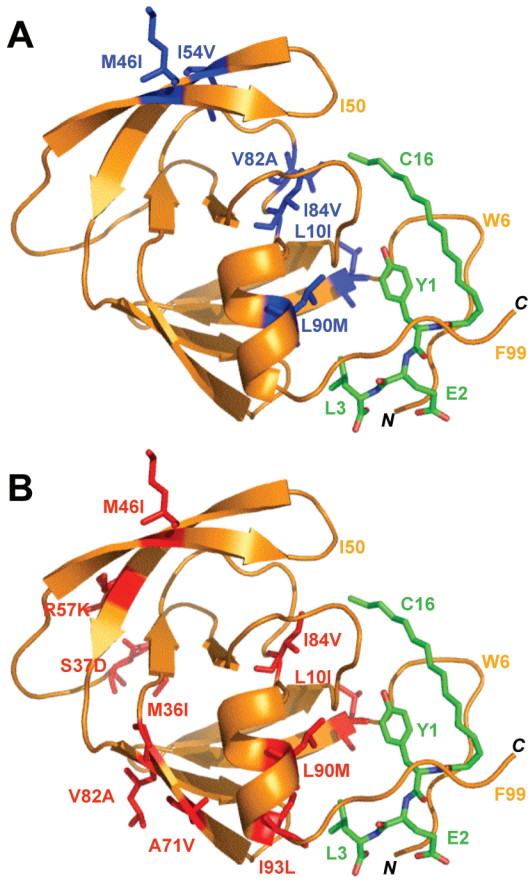

FIGURE 6: Models of an alkyl peptide associated to MDR-HM and ANAM-11 HIV-1 proteases. Alkyl chains do not interact with mutated side chains in drug-resistant mutated HIV-1 proteases MDR-HM (A) and ANAM-11 (B). Mutations are indicated in blue (MDR-HM) and red (ANAM-11) in the 90° side view of the C16-YEL (sticks)/monomer (orange sketch) complexes.

approved PIs tipranavir and darunavir target the HIV-PR active site and were also described to disrupt dimers from two-hybrid and FRET experiments (*42*). Darunavir interacts with D^{29} involved in the key intermolecular ion pair D^{29}-R^{8}, and this interaction is maintained in mutated HIV-1 proteases (*43*). Three-fourths of the dimer association free energy is ensured by the intermolecular β-sheet not involved with the active site (*13*). Thus we focused this study on the rational design of lipopeptides that target this intermolecular β-sheet. We have demonstrated by analytical ultracentrifugation that their inhibitory action is due to disruption of PR dimers and monomer sequestration. Sedimentation velocity experiments showed that HIV-PR homodimer in the absence of C16-YEL and the monomer/C16-YEL complex are single species, and equilibrium sedimentation experiments confirm the molecular weight of these species. Kinetic analyses and molecular modeling helped us, by comparison of lipopeptide series, to analyze and describe the respective roles of alkyl and peptide parts. The peptide moiety specifically targets the intermolecular antiparallel β-sheet away from the active site, whereas the hydrophobic alkyl chain is grasped by the protease hydrophobic cleft, thus burying the hydrophobic side chains that form the dimer interface. Long alkyl chains also mask catalytic residues. Alkyl tripeptides are easy to synthesize, and C16-LEY is one of the most potent inhibitors ever tested by kinetics (K_{id} = 0.3 nM). The arrangement of peptides within the HIV-PR β-sheet was consistent with NMR studies using the dimerization inhibitor Ac-SYEL (*41*) and the design of molecular tongs in which two interface peptides were cross-linked with a rigid spacer (*28*−*30*) constraining backbone orientations and distance. We also explored the possibilities to substitute in these tongs any amino acids by peptidomimetic motifs (*30*). Flexible spacers have also been reported to link interfacial peptides (*14, 17, 31*), but all of these cross-linked peptides or peptidomimetics were less efficient than the alkyl peptides described in this work.

Our alkyl tripeptide inhibitors are also effective against mutated proteases that retain their potency *in vitro*, whereas clinical protease inhibitors targeting the active site are ineffective. Mutations of the enzyme in drug-resistant HIV-1 virus strains do not significantly alter steric hindrance in the lipopeptide alkyl chain binding site or in the hydrophobic pocket fitting the amino acid at the third position. Our models suggest that any mutation that places bulky or hydrophilic side chains in the hydrophobic cleft or F^{B99} pocket should weaken lipopeptide binding and also PR dimer formation, leading to an inactive PR and defective virus. These alkyl tripeptides that disrupt HIV-1 protease dimerization are likely to remain active against HIV strains that are resistant to "classical" PIs.

ACKNOWLEDGMENT

The authors thank Prof. Ernesto Freire of the Department of Biology and Biocalorimetry Center, The Johns Hopkins University, Baltimore, MD, for the generous gift of plasmids encoding MDR-HM and ANAM-11 mutants. We thank Dr. Owen Parkes for assistance with the English text.

SUPPORTING INFORMATION AVAILABLE

Detailed information about the inhibitor synthesis and stability tests performed in this work (SD1), structure schemes of alkyl tripeptides (SD2), sedimentation equilibrium of C16-LEY/HIV-PR and C12-YEL/HIV-PR (SD3), detailed procedure of molecular modeling (SD4), and interface areas calculated from models of alkyl peptide/HIV-PR complexes (SD5). This material is available free of charge via the Internet at http://pubs.acs.org.

REFERENCES

1. Kohl, N. E., Emini, E. A., Schleif, W. A., Davis, L. J., Heimbach, J. C., Dixon, R. A., Scolnick, E. M., and Sigal, I. S. (1988) Active human immunodeficiency virus protease is required for viral infectivity. *Proc. Natl. Acad. Sci. U.S.A. 85*, 4686–4690.
2. Peng, C., Ho, B. K., Chang, T. W., and Chang, N. T. (1989) Role of human immunodeficiency virus type 1-specific protease in core protein maturation and viral infectivity. *J. Virol. 63*, 2550–2556.
3. Carr, A. (2003) Toxicity of antiretroviral therapy and implications for drug development. *Nat. Rev. Drug Discov. 2*, 624–634.
4. De Clercq, E. (2004) Antivirals and antiviral strategies. *Nat. Rev. Microbiol. 2*, 704–720.
5. Wells, J. A., and McClendon, C. L. (2007) Reaching for high-hanging fruit in drug discovery at protein-protein interfaces. *Nature 450*, 1001–1009.
6. Wlodawer, A., Miller, M., Jaskolski, M., Sathyanarayana, B. K., Baldwin, E., Weber, I. T., Selk, L. M., Clawson, L., Schneider, J., and Kent, S. B. (1989) Conserved folding in retroviral proteases: crystal structure of a synthetic HIV-1 protease. *Science 245*, 616–621.
7. Spinelli, S., Liu, Q. Z., Alzari, P. M., Hirel, P. H., and Poljak, R. J. (1991) The three-dimensional structure of the aspartyl protease from the HIV-1 isolate BRU. *Biochimie 73*, 1391–1396.
8. Hong, L., Hartsuck, J. A., Foundling, S., Ermolieff, J., and Tang, J. (1998) Active-site mobility in human immunodeficiency virus,

type 1, protease as demonstrated by crystal structure of A28S mutant. *Protein Sci. 7*, 300–305.
9. Hamelberg, D., and McCammon, J. A. (2005) Fast peptidyl cis-trans isomerization within the flexible Gly-rich flaps of HIV-1 protease. *J. Am. Chem. Soc. 127*, 13778–13779.
10. Hornak, V., Okur, A., Rizzo, R. C., and Simmerling, C. (2006) HIV-1 protease flaps spontaneously open and reclose in molecular dynamics simulations. *Proc. Natl. Acad. Sci. U.S.A. 103*, 915–920.
11. Ding, F., Layten, M., and Simmerling, C. (2008) Solution structure of HIV-1 protease flaps probed by comparison of molecular dynamics simulation ensembles and EPR experiments. *J. Am. Chem. Soc. 130*, 7184–7185.
12. Sayer, J. M., Liu, F., Ishima, R., Weber, I. T., and Louis, J. M. (2008) Effect of the active site D25N mutation on the structure, stability, and ligand binding of the mature HIV-1 protease. *J. Biol. Chem. 283*, 13459–13470.
13. Todd, M. J., Semo, N., and Freire, E. (1998) The structural stability of the HIV-1 protease. *J. Mol. Biol. 283*, 475–488.
14. Zutshi, R., Franciskokovich, J., Shultz, M., Schweitzer, B., Bishop, P., Wilson, M., and Chmielewski, J. (1997) Targeting the dimerization interface of HIV-1 protease: inhibition with cross-linked interfacial peptides. *J. Am. Chem. Soc. 119*, 4841–4845.
15. Boggetto, N., and Reboud-Ravaux, M. (2002) Dimerization inhibitors of HIV-1 protease. *Biol. Chem. 383*, 1321–1324.
16. Bannwarth, L., and Reboud-Ravaux, M. (2007) An alternative strategy for inhibiting multidrug-resistant mutants of the dimeric HIV-1 protease by targeting the subunit interface. *Biochem. Soc. Trans. 35*, 551–554.
17. Bowman, M. J., and Chmielewski, J. (2008) Sidechain-linked inhibitors of HIV-1 protease dimerization. *Bioorg. Med. Chem.* (doi: 10.1016/j.bmc.2008.02.060).
18. Findeis, M. A., and Molineaux, S. M. (1999) Design and testing of inhibitors of fibril formation. *Methods Enzymol. 309*, 476–488.
19. Nakagami, Y., Nishimura, S., Murasugi, T., Kaneko, I., Meguro, M., Marumoto, S., Kogen, H., Koyama, K., and Oda, T. (2002) A novel beta-sheet breaker, RS-0406, reverses amyloid beta-induced cytotoxicity and impairment of long-term potentiation in vitro. *Br. J. Pharmacol. 137*, 676–682.
20. Pinkner, J. S., Remaut, H., Buelens, F., Miller, E., Aberg, V., Pemberton, N., Hedenstrom, M., Larsson, A., Seed, P., Waksman, G., Hultgren, S. J., and Almqvist, F. (2006) Rationally designed small compounds inhibit pilus biogenesis in uropathogenic bacteria. *Proc. Natl. Acad. Sci. U.S.A. 103*, 17897–17902.
21. Schramm, H. J., Nakashima, H., Schramm, W., Wakayama, H., and Yamamoto, N. (1991) HIV-1 reproduction is inhibited by peptides derived frm the N- and C-termini of HIV-1 protease. *Biochem. Biophys. Res. Commun. 179*, 847–851.
22. Franciskovich, J., Houseman, K., Mueller, R., and Chmielewski, J. A. (1993) *Bioorg. Med. Chem. Lett. 3*, 765–768.
23. Schramm, H. J., Boetzel, J., Buttner, J., Fritsche, E., Gohring, W., Jaeger, E., Konig, S., Thumfart, O., Wenger, T., Nagel, N. E., and Schramm, W. (1996) The inhibition of human immunodeficiency virus proteases by "interface peptides". *Antiviral Res. 30*, 155–170.
24. Schramm, H. J., de Rosny, E., Reboud-Ravaux, M., Buttner, J., Dick, A., and Schramm, W. (1999) Lipopeptides as dimerization inhibitors of HIV-1 protease. *Biol. Chem. 380*, 593–596.
25. Dumond, J., Boggetto, N., Schramm, H. J., Schramm, W., Takahashi, M., and Reboud-Ravaux, M. (2003) Thyroxine-derivatives of lipopeptides: bifunctional dimerization inhibitors of human immunodeficiency virus-1 protease. *Biochem. Pharmacol. 65*, 1097–1102.
26. Petry, H., Ast, E., De Rosny, E., Jentsch, K.-D., Hunsmann, G., Goldmann, C., Lüke, W., Büttner, J., Reboud, M., Schramm, W., and Schramm, H. J. (1999) *HIV-Infekt*, Springer, Paris, France.
27. Breccia, P., Boggetto, N., Perez-Fernandez, R., Van Gool, M., Takahashi, M., Rene, L., Prados, P., Badet, B., Reboud-Ravaux, M., and de Mendoza, J. (2003) Dimerization inhibitors of HIV-1 protease based on a bicyclic guanidinium subunit. *J. Med. Chem. 46*, 5196–5207.
28. Bouras, A., Boggetto, N., Benatalah, Z., de Rosny, E., Sicsic, S., and Reboud-Ravaux, M. (1999) Design, synthesis, and evaluation of conformationally constrained tongs, new inhibitors of HIV-1 protease dimerization. *J. Med. Chem. 42*, 957–962.
29. Merabet, N., Dumond, J., Collinet, B., Van Baelinghem, L., Boggetto, N., Ongeri, S., Ressad, F., Reboud-Ravaux, M., and Sicsic, S. (2004) New constrained "molecular tongs" designed to dissociate HIV-1 protease dimer. *J. Med. Chem. 47*, 6392–6400.
30. Bannwarth, L., Kessler, A., Pethe, S., Collinet, B., Merabet, N., Boggetto, N., Sicsic, S., Reboud-Ravaux, M., and Ongeri, S. (2006) Molecular tongs containing amino acid mimetic fragments: new inhibitors of wild-type and mutated HIV-1 protease dimerization. *J. Med. Chem. 49*, 4657–4664.
31. Bowman, M. J., and Chmielewski, J. (2002) Novel strategies for targeting the dimerization interface of HIV protease with cross-linked interfacial peptides. *Biopolymers 66*, 126–133.
32. Neimark, J., and Briand, J. P. (1993) Development of a fully automated multichannel peptide synthesizer with integrated TFA cleavage capability. *Pept. Res. 6*, 219–228.
33. Ohtaka, H., Schon, A., and Freire, E. (2003) Multidrug resistance to HIV-1 protease inhibition requires cooperative coupling between distal mutations. *Biochemistry 42*, 13659–13666.
34. Muzammil, S., Ross, P., and Freire, E. (2003) A major role for a set of non-active site mutations in the development of HIV-1 protease drug resistance. *Biochemistry 42*, 631–638.
35. Billich, A., Hammerschmid, F., and Winkler, G. (1990) Purification, assay and kinetic features of HIV-1 proteinase. *Biol. Chem. Hoppe-Seyler 371*, 265–272.
36. Szeltner, Z., and Polgar, L. (1996) Conformational stability and catalytic activity of HIV-1 protease are both enhanced at high salt concentration. *J. Biol. Chem. 271*, 5458–5463.
37. Zhang, Z. Y., Poorman, R. A., Maggiora, L. L., Heinrikson, R. L., and Kezdy, F. J. (1991) Dissociative inhibition of dimeric enzymes. Kinetic characterization of the inhibition of HIV-1 protease by its COOH-terminal tetrapeptide. *J. Biol. Chem. 266*, 15591–15594.
38. Schuck, P. (2000) Size-distribution analysis of macromolecules by sedimentation velocity ultracentrifugation and lamm equation modeling. *Biophys. J. 78*, 1606–1619.
39. Lindahl, E., Azuara, C., Koehl, P., and Delarue, M. (2006) NOMAD-Ref: visualization, deformation and refinement of macromolecular structures based on all-atom normal mode analysis. *Nucleic Acids Res. 34*, W52–W56.
40. Louis, J. M., Wondrak, E. M., Kimmel, A. R., Wingfield, P. T., and Nashed, N. T. (1999) Proteolytic processing of HIV-1 protease precursor, kinetics and mechanism. *J. Biol. Chem. 274*, 23437–23442.
41. Frutos, S., Rodriguez-Mias, R. A., Madurga, S., Collinet, B., Reboud-Ravaux, M., Ludevid, D., and Giralt, E. (2007) Disruption of the HIV-1 protease dimer with interface peptides: structural studies using NMR spectroscopy combined with [2-(13)C]-Trp selective labeling. *Biopolymers 88*, 164–173.
42. Koh, Y., Matsumi, S., Das, D., Amano, M., Davis, D. A., Li, J., Leschenko, S., Baldridge, A., Shioda, T., Yarchoan, R., Ghosh, A. K., and Mitsuya, H. (2007) Potent inhibition of HIV-1 replication by novel non-peptidyl small molecule inhibitors of protease dimerization. *J. Biol. Chem. 282*, 28709–28720.
43. Muzammil, S., Armstrong, A. A., Kang, L. W., Jakalian, A., Bonneau, P. R., Schmelmer, V., Amzel, L. M., and Freire, E. (2007) Unique thermodynamic response of tipranavir to human immunodeficiency virus type 1 protease drug resistance mutations. *J. Virol. 81*, 5144–5154.

BI801422U